The fate of particles in a volumetrically heated convective fluid at high Prandtl number – Supplementary Material

Cyril Sturtz, Édouard Kaminski, Angela Limare and Stephen Tait

1 Experimental apparatus

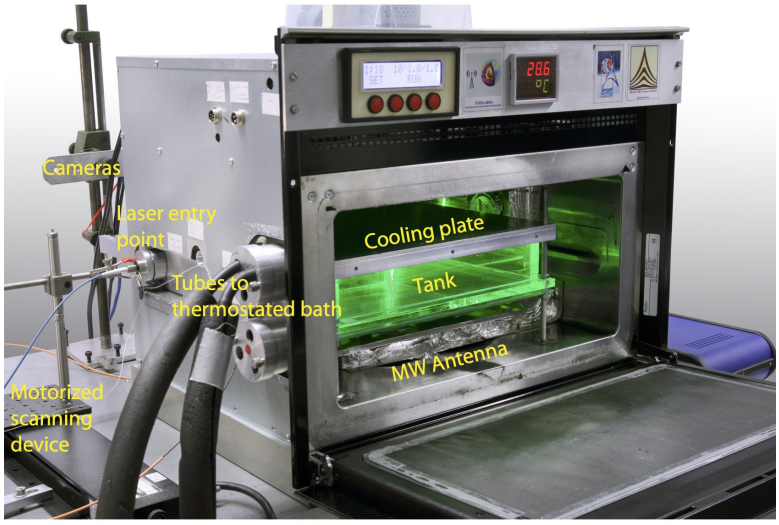

FIGURE 1 – Picture of the setup used in this study (taken from Limare et al. [2019]).

2 Properties of fluids and beads – methods

2.1 Fluid

The fluid used in this study is a mixture of 44wt% glycerol and 56wt% ethylene glycol. Density and thermal expansion have been determined thanks to a DMA 5000 Anton Paar densimeter. Thermal properties, such as thermal diffusivity κ_f, thermal conductivity λ_f and specific heat $c_{p,f}$, have been determined thanks to a photothermal method described by Dadarlat and Neamtu [2009]. The viscosity η_f and its dependance on temperature have been monitored thanks to an RS600 Anton Paar rheometer. The refractive index n_f and its temperature dependence have been obtained thanks to the Abbemat 350 Anton Paar refractometer. These properties are shown in table 1 and their tempertaure dependence is plotted in figure 2 (a), (b) and (c).

2.2 Beads

As beads are small solid spheres, the measure of previous properties is much more complicated. To measure the density, we introduced the beads in a tank containing a stratified fluid. This density stratification is achieved by the double bucket method described by Fortuin [1960] and illustrated in figure 3. The buckets contain two mixtures of different proportions of water and glycerol having different densities, called (A) and (B) for the high and low value respectively. As the heavy mixture (A) is pumped into the working tank (S), the lighter one (B) is introduced in (A) thanks to a basal linking tube, reducing the density of (A) and, hence, the density of the fluid deposed in the tank (S). Step by step, as the pumping is going on, the density of fluid introduced in (S) becomes less important. The stratification so created is sampled at different heights, and controlled apart, thanks to the DMA 5000 Anton Paar densimeter. Beads are introduced in the stratified liquid, and they stop at a level corresponding to their neutral buoyancy heigh (NBH). The determination of this height is a way to measure their density.

In order to measure the thermal expansion α_p, this type of set up has been carried on for different thermostated environments. Achieving a stable and isothermal stratified environment is extremely complicated, because even a difference of a few degrees between the wall of the tank and the bulk might trigger convection, and thus, destroy the stratification. In order to prevent this effect, the fluids (A) and (B) have been prepared in a thermostated room, whose temperature can be tuned within a certain range (between 18 and 27^{o}C). In this way, we get three measurements of density at three different temperatures (Figure 2 (a)), and assuming a constant thermal expansion, we get the following value for beads : $\alpha_p = 3.17.10^{-4}$ K^{-1}.

We work with two families of beads of different radius. Their size has been determined by image analysis of a sample of hundreds of beads of each family. The size distribution is plotted in Figure 2 (d), and it leads to the estimation of the averaged radius : $r_1 = 290$ μm and $r_2 = 145$ μm.

All the other thermal properties are taken in Mark [2007] : $\lambda_p = 0.21$ W/m/K, $c_{p,p} = 1765$ J/kg/K and thus $\kappa_p = 1.10^{-7}$ m^2/s. Concerning the refractive index, the handbook exposes a wide range of values, from 1.445 for bead to 1.56 (Mark [2007], p.830). As we noticed a strong index mismatch in experiments, the refractive index of the beads is likely to be closer to the upper bound of this range.

3 How to introduce beads without bubbles ?

Achieving an appropriate experimental setup that involves a fluid bearing beads is actually challenging. Especially, we have to avoid introducing air bubbles in the mush, as it might induce unwanted surface tension effects, and, thus, increase cohesion between particles.

To do so, we systematically applied the following protocol. First, the working tank is filled with the fluid. Then, we prepared a mixture of fluid and beads in the home-made stir-machine – see Figure 5 (a) and (b). The stir-machine includes a vessel and a rotor that is composed of an horizontal grid aiming to maintain the beads in the lower part of the stir-machine, and let

Properties	Symbol	Value
Fluid density (20^oC)	$\rho_{0,p}$	1192 kg.m^{-3}
Beads density (20^oC)	$\rho_{0,p}$	1187 kg.m^{-3}
Fluid thermal expansion	α_f	5.5 10^{-4} K^{-1}
Beads thermal expansion	α_p	3.2 10^{-4} K^{-1}
Fluid viscosity (20^oC)	η_f	0.151 Pa.s
Activation energy	E_a	41.7 kJ.mol^{-1}
Fluid thermal diffusion coefficient	κ_f	9.1 10^{-8} m^2.s^{-1}
Beads thermal diffusion coefficient(*)	κ_p	1. 10^{-7} m^2.s^{-1}
Fluid thermal conductivity	λ_f	0.276 W.m^{-1}.K^{-1}
Beads thermal conductivity(*)	λ_p	0.21 W.m^{-1}.K^{-1}

TABLE 1 – Main physical properties of the fluid and beads. The activation energy corresponds to the fit of the variation of viscosity with an Arrhenius law. Properties are all measured, except those marked with (*) which are taken from Mark [2007].

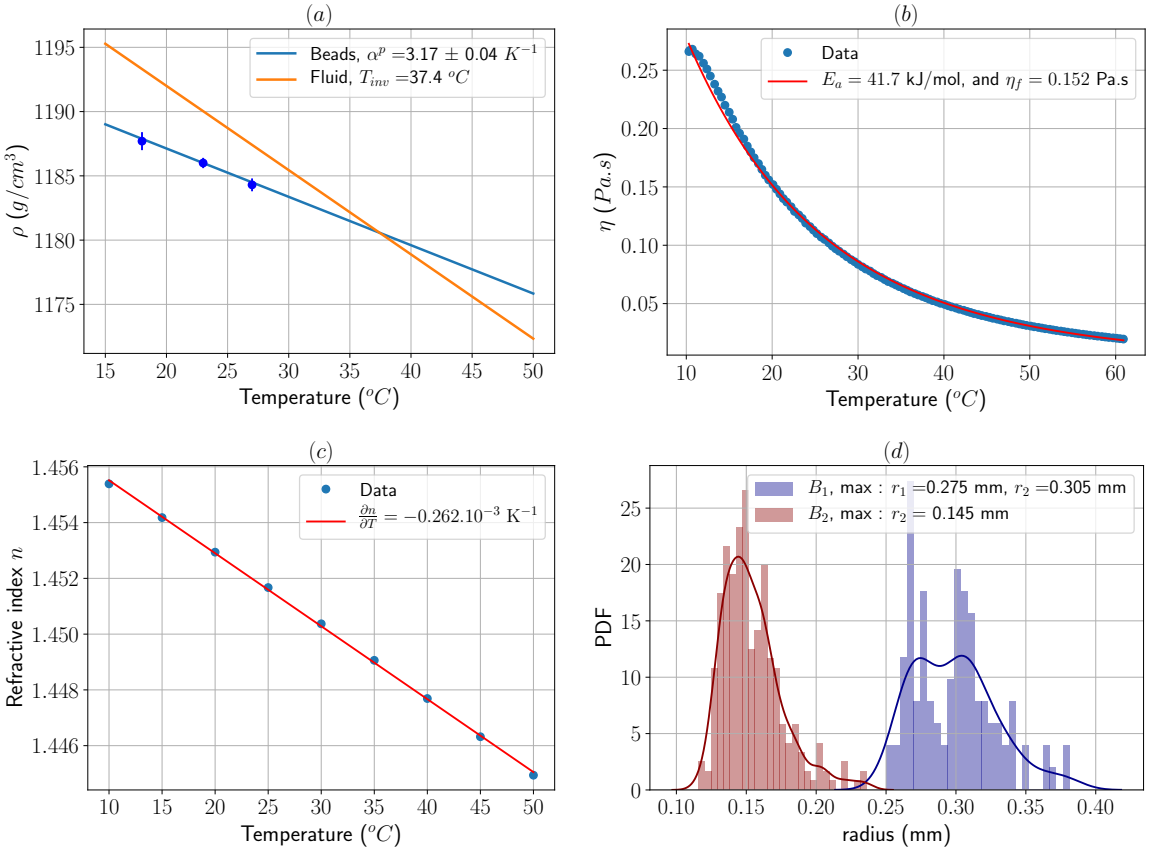

FIGURE 2 – Some properties of the fluid and beads that has been measured. (a) : fluid and beads density. Blue dots represent experiments using thermalised stratifications and are described in the text. (b) : Fluid viscosity as a function of the temperature. The fit represents an ARRHENIUS law : $\eta(T) = \eta_f \exp\left[\frac{E_a}{R}\left(\frac{1}{T} - \frac{1}{T_0}\right)\right]$ with $T_0 = 20^oC$. (c) : fluid refractive index as a function of the temperature. (d) : beads radius distribution.

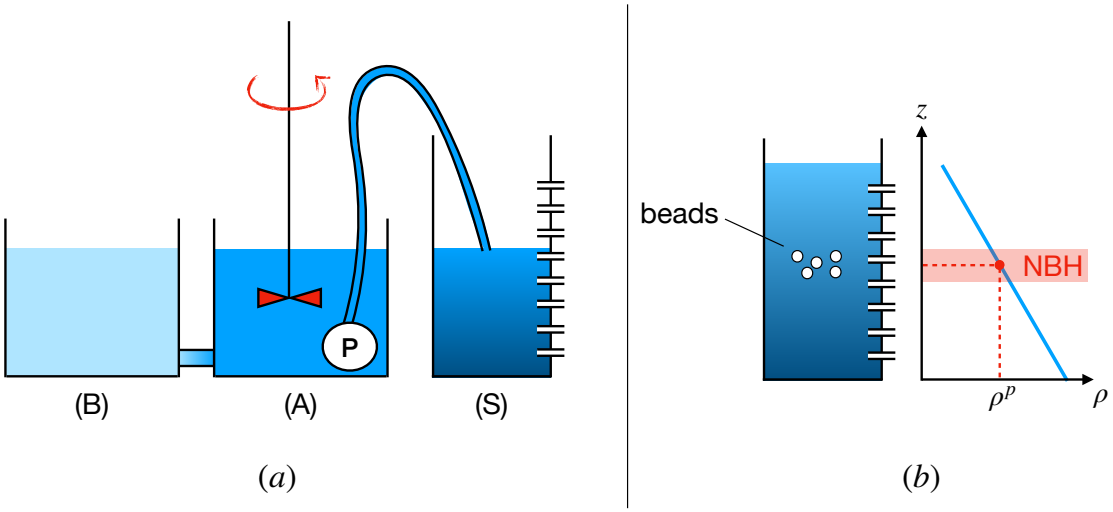

FIGURE 3 – (a) : Setup to create a stratified environment (S), using the double-bucket method. The density stratification created in (S) is measured by sampling the liquid in the tank at different heights, as represented at the right wall of (S). (b) : scheme showing the measurement of beads density by the determination of their neutral buoyancy height (NBH).

the bubbles escape. This protocol is done at room temperature, therefore beads float and form a lid against the grid. In order to prevent settling and to maintain the beads in suspension, three blades are also attached to the rotating grid. Degassing the mixture consists in stirring the fluid with beads, and letting it quiescent in order to let the bubbles escape. This procedure is repeated several times, until no more bubbles escaped from the separation grid. Then, the stir-machine is connected to the working tank. Isostatic pressure enables the beads to go from the stir-machine to the tank. The flow has to be controlled in order not to let particles be entrained and escape the working tank. Once the amount of particles introduced is sufficient, the tank is closed, shaken to homogenize the mixture, and placed into the oven. We waited until particles settle before beginning any experiment. The total beads mass introduced in the tank is measured at the end of the set of experiments, when the tank is drained, the mixture is sieved, and the beads are washed, dried and then weighed.

4 Snapshots of the top and bottom deposits

Figure 5 shows two pictures of the deposits studied : (a) the floating crust that forms at the surface, and (b) the cumulate that appears when some conditions enable its formation. Picture (a) has been taken at the end of an experiment, when all particles have settled at the surface. Note the egg-box-like shape of the floating lid, very similar to shape that can be observed in geomorphology and in experiments by Solomatov et al. [1993]. Concerning the basal cumulate (d), note that deposits form patterns like dunes. We must emphasize that these dunes move and deform as the convection goes on.

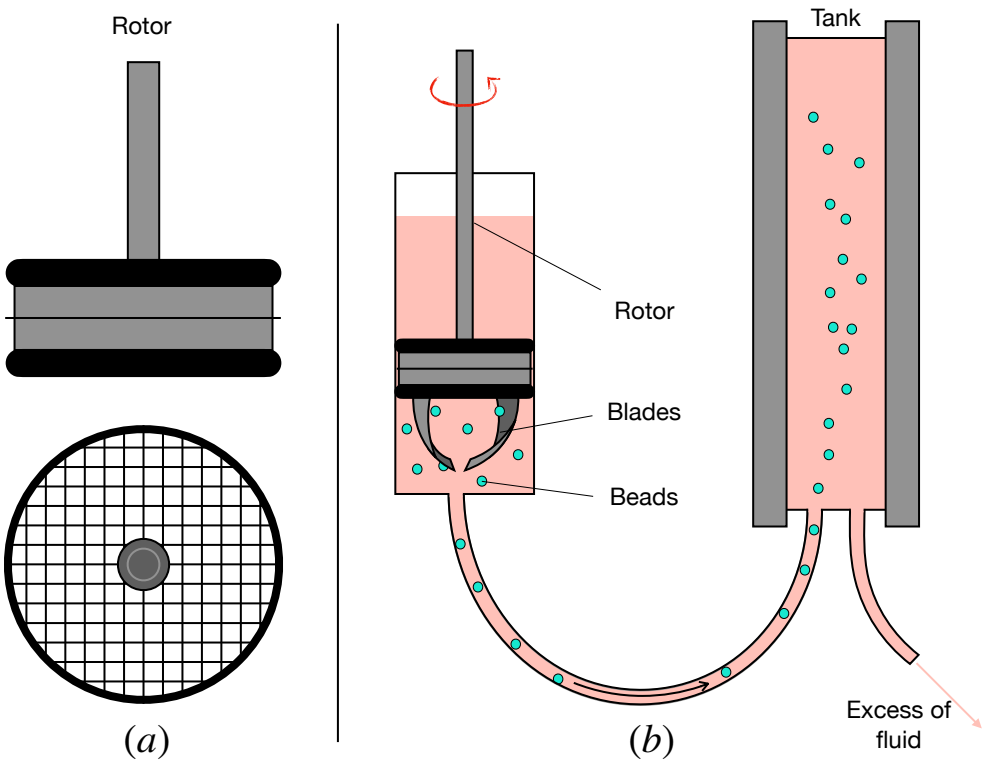

FIGURE 4 – Stir-machine that enables the introduction of beads without air bubbles. (a) The grid in the rotor has a mesh smaller than the beads diameter, that retains them in the lower part of the cylinder while letting the bubbles escape. (b) Set up to introduce beads in the tank in the vertical position. The grid and the rotor are immersed in the fluid. Blades have also been fixed on the rotor, in order to keep beads in suspension, to avoid their settling against the grid and to allow bubbles detachment and escape through the grid.

(*a*)

(*b*)

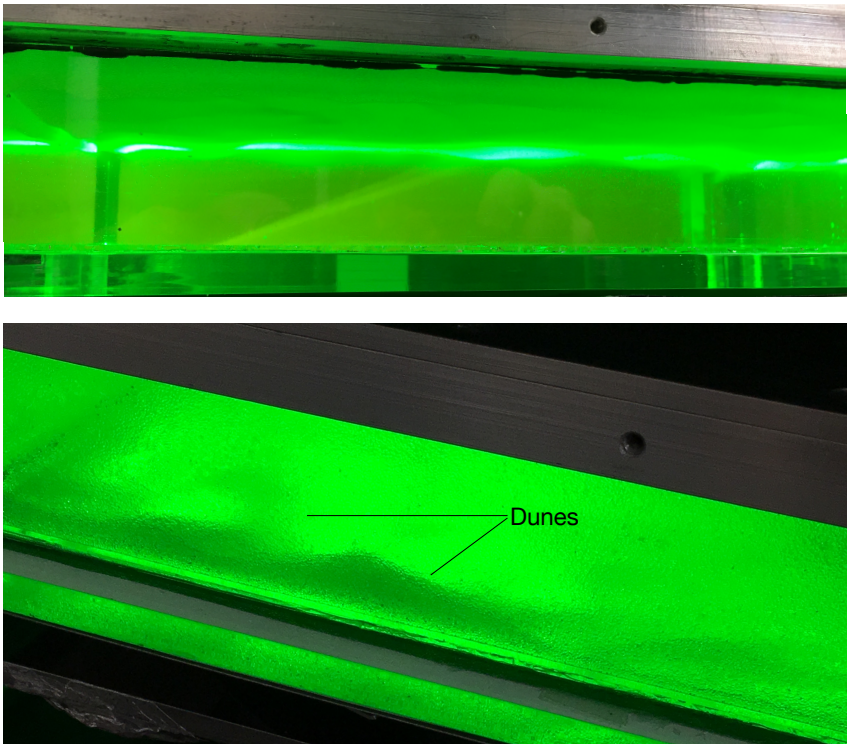

FIGURE 5 – Different types of deposits that can form during experiments. (*a*) : picture of settled beads at room temperature. (*b*) : snapshot of the cumulate forming at the end of a hot experiment. Note that both deposits are dune-shaped.

5 Data for the scaling laws dealing with strain rates and velocities

Refractive index mismatch between the fluid and beads affected the velocity field as soon as the laser sheet scanned larger distances from the front wall and the concentration of particles became significant. We performed 8 experiments without any beads in order to determine accurately the scaling laws for the velocity and the strain rate. We measured the steady-state velocity field in order to calculate either the characteristic velocities (vertical and horizontal) and the characteristic strain rate (vertical and horizontal). All these values are evaluated by their root mean square (RMS) values calculated over the entire volume of the tank. The results are shown in Table 2. These data were used to determine the scaling laws shown in section 4.2.2.

Name	Ra_H (10^7)	T_s (^oC)	T_{bulk} (^oC)	U_x (10^{-4} m/s)	U_z (10^{-4} m/s)	$\dot{\gamma}_{xz}$ (10^{-2}/s)	$\dot{\gamma}_{zx}$ (10^{-2}/s)
IHB29_1	0.28	22.2	26.0	2.64	2.64	4.21	4.19
IHB29_2	3.4	22.2	34.5	7.96	7.48	13.7	14.8
IHB29_3	7.9	22.3	38.9	6.26	6.11	10.3	11.6
IHB30_1	0.77	22.3	28.5	3.72	3.64	5.77	6.00
IHB30_2	1.8	22.4	31.4	5.09	4.50	7.69	7.64
IHB30_3	12.2	25.6	43.1	7.68	6.66	16.2	16.3
IHB31_1	0.16	9.1	16.5	2.29	1.76	4.28	3.66
IHB31_2	13.3	29.4	46.6	10.0	8.83	18.6	19.7

TABLE 2 – Experimental conditions (steady-state Ra_H and surface and bulk temperatures T_s and T_{bulk} respectively) and RMS values of the horizontal velocity (U_x), vertical velocity (U_z), horizontal strain rate ($\dot{\gamma}_{xz}$) and vertical strain rate ($\dot{\gamma}_{zx}$), obtained in homogeneous, beads-free experiments.

Références

A. Limare, C. Jaupart, E. Kaminski, L. Fourel, and C.G. Farnetani. Convection in an internally heated stratified heterogeneous reservoir. *Journal of Fluid Mechanics*, 870 :67–105, 2019. doi : 10.1017/jfm.2019.243.

D. Dadarlat and C. Neamtu. High performance photopyroelectric calorimetry of liquids. *Acta Chim. Slov*, 56 :225–236, 01 2009.

J.M.H. Fortuin. Theory and application of two supplementary methods of constructing density gradient contrast. *Journal of Polymer Science*, 44(144) :505–515, 1960. doi : 10.1002/pol.1960.1204414421.

J.E. Mark, editor. *Physical Properties of Polymers Handbook, 2nd edition*, volume 29. Springer, 2007. ISBN 978-0-387-31235-4. doi : 10.1007/978-0-387-69002-5.

V.S. Solomatov, P. Olson, and D.J. Stevenson. Entrainment from a bed of particles by thermal convection. *Earth and Planetary Science Letters*, 120(3) :387 – 393, 1993. ISSN 0012-821X. doi : https://doi.org/10.1016/0012-821X(93)90252-5. URL `http://www.sciencedirect.com/science/article/pii/0012821X93902525`.